

Spin Determination for Fermiophobic Bosons

Jason Kumar,¹ Arvind Rajaraman,² and David Yaylali¹

¹*Department of Physics and Astronomy,
University of Hawai'i, Honolulu, HI 96822, USA*

²*Department of Physics and Astronomy,
University of California, Irvine, CA 92697*

Abstract

We discuss the prospects for production and detection of fermiophobic bosons (exotic bosons decaying only to standard model gauge bosons) at the LHC, and describe simple methods for determining spin. We consider two complementary approaches to spin determination: the search for decays in the diphoton channel, and the comparison of events with no extra spectator jets to those with one extra jet. We show that these approaches can together allow the fermiophobic boson's spin to be determined over a wide range of parameter space. We study both even and odd parity states.

PACS numbers: 12.60.-i, 14.70.Pw

I. INTRODUCTION

In this paper we will study the phenomenology of massive fermiophobic bosons (denoted throughout this paper as X). Fermiophobic bosons dominantly couple to standard model gauge-bosons. We consider possible strategies for distinguishing a spin-0 fermiophobic resonance from a spin-1 resonance (we consider both even and odd parity). We will find that there are two effective complementary strategies: a search for diphoton events, and a comparison of events with no spectator jets to those with one spectator jet.

Fermiophobic bosons have been studied in a variety of contexts [1–13], particularly in the context of a fermiophobic Higgs boson [14]. Fermiophobic bosons can arise naturally in models where a hidden sector couples dominantly to exotic heavy fermions or scalars. If these matter fields are heavy enough, then they cannot be directly produced at the LHC. But if these fields are charged under standard model gauge groups, then loops of heavy particles mediate an effective coupling to standard model gauge bosons. One-loop diagrams can thus mediate mixing between standard model gauge bosons and fermiophobic bosons, and search strategies for this effect have been well-studied [1–3, 5–9]. An alternative strategy is to search for triple-boson couplings, where X couples to two standard model gauge bosons. This strategy can be especially useful in cases where X does not mix with standard model gauge bosons; examples include the case where X is a scalar, or when the heavy fields mediating the interaction are not charged under $U(1)_Y$.

One would expect that the most effective way to search for fermiophobic bosons with triple boson couplings would be through the process $gg \rightarrow X \rightarrow VV$, where V is an electroweak gauge boson. This process benefits from large production rate associated with a gluon initial state, and clean photon or lepton signals which are possible with an electroweak boson final state. This channel was studied in [12] for the case where X is a pseudovector. A variety of experimental searches for fermiophobic bosons have been conducted [15].

It is important to determine all quantum numbers of any exotic resonance discovered at the LHC. The measurement of the spin of a resonance has been studied by many authors, particularly in the context of resonances similar to the Higgs [16]. A typical method of spin determination is to look at the angular distribution of the decay products in the rest frame of the decaying particle. We will consider two complementary approaches to spin determination which do not require the use of angular information, but instead rely on effects associated with Landau-Yang theorem [17, 18] selection rules.

According to the Landau-Yang theorem, a massive vector boson cannot decay to two identical massless vector bosons. Thus, if the decay $X \rightarrow \gamma\gamma$ is observed, it is clear that X is not spin-1. This is the reason why it is clear that the recent exciting discovery at the LHC of a boson with a mass of ~ 125 GeV [19] cannot be a spin-1 resonance. The Landau-Yang theorem also implies that a massive vector cannot be produced from an initial state of two on-shell gluons. This implies that the production of a spin-1 fermiophobic boson from an Xgg vertex must be accompanied by the emission of a spectator jet. We will find that these two strategies can be used together to distinguish between spin-0 and spin-1 fermiophobic bosons for a wide range of models. The efficacy of each strategy depends primarily on the relative strength of the coupling of X to $SU(2)$ and to $U(1)_Y$ gauge bosons.

In section II, we describe the coupling of fermiophobic bosons to standard model gauge bosons in terms of higher-dimension effective operators. In section III we describe the primary X production and decay processes. In section IV we describe our method of simulating signal and background events, and in section V we describe the sensitivity of the LHC, and

its ability to distinguish the spin of fermiophobic resonances. We conclude in section VI with a discussion of our results.

II. EFFECTIVE THEORY OF THE FERMIOPHOBIC BOSON

The theory we consider consists of a new massive boson X which has effective couplings to standard model gauge bosons. We will assume X is not charged under standard model gauge groups; the coupling can thus be written as an effective operator of dimension 5 or 6 (depending on the spin of X) which couples X to standard model field strengths. We now list the possible (lowest dimensional) effective operators for the four spin/parity assignments of this boson.

For either a scalar or pseudoscalar, there is one lowest dimension (dimension 5) effective operator.

$$\mathcal{O}_s = \frac{1}{\Lambda} X \text{Tr}[F_{\mu\nu} F^{\mu\nu}], \quad (1)$$

$$\mathcal{O}_{ps} = \frac{1}{\Lambda} \epsilon_{\alpha\beta\gamma\delta} X \text{Tr}[F^{\alpha\beta} F^{\gamma\delta}]. \quad (2)$$

For a (pseudo)vector X , the lowest dimensional operator is of dimension 6. For the vector, we find four possible operators:

$$\mathcal{O}_v^1 = \frac{1}{\Lambda^2} X^\mu \text{Tr}[F_{\mu\alpha} \partial_\beta F^{\alpha\beta}] \quad (3)$$

$$\mathcal{O}_v^2 = \frac{1}{\Lambda^2} X^\mu \text{Tr}[\partial_\beta F_{\mu\alpha} F^{\alpha\beta}] \quad (4)$$

$$\mathcal{O}_v^3 = \frac{1}{\Lambda^2} \partial_\beta X^\mu \text{Tr}[F_{\mu\alpha} F^{\alpha\beta}] \quad (5)$$

$$\mathcal{O}_v^4 = \frac{1}{\Lambda^2} X^\mu \text{Tr}[F_{\alpha\beta} \partial_\mu F^{\alpha\beta}], \quad (6)$$

where we have written each operator only to quadratic order in standard model gauge field strengths. For a fully gauge-invariant operator, the partial derivative should be replaced by a covariant derivative. The first three operators are related by an integration by parts.

$$X^\mu \text{Tr}[F_{\mu\alpha} \partial_\beta F^{\alpha\beta}] = \partial_\beta (X^\mu \text{Tr}[F_{\mu\alpha} F^{\alpha\beta}]) - (X^\mu \text{Tr}[\partial_\beta F_{\mu\alpha} F^{\alpha\beta}] + \partial_\beta X^\mu \text{Tr}[F_{\mu\alpha} F^{\alpha\beta}]).$$

Dropping the surface term, we find

$$\mathcal{O}_v^1 \sim -(\mathcal{O}_v^2 + \mathcal{O}_v^3).$$

We will in what follows assume X to be on-shell. In this case, we find that the operator \mathcal{O}_v^2 does not contribute. The vertex function for this operator is

$$\begin{aligned} \Gamma_{v(2)}^{\mu\nu\rho}(k_X, k_1, k_2) &= \frac{1}{\Lambda^2} (k_1^\mu + k_2^\mu) (k_1^\rho k_2^\nu - g^{\rho\nu} k_1 \cdot k_2) \\ &= \frac{1}{\Lambda^2} k_X^\mu (k_1^\rho k_2^\nu - g^{\rho\nu} k_1 \cdot k_2). \end{aligned} \quad (7)$$

Contracting this vertex function with the polarization vector for the X thus gives zero. The vertex function for \mathcal{O}_v^4 is identical, and so also does not contribute. Thus the only operators

which contribute to the X coupling are \mathcal{O}_v^1 and \mathcal{O}_v^3 , which are equivalent by an integration by parts. We thus drop superscript labels and write

$$\mathcal{O}_v = \frac{1}{\Lambda^2} X^\mu \text{Tr}[F_{\mu\alpha} \partial_\beta F^{\alpha\beta}]. \quad (8)$$

Finally, for the pseudovector X , the only non-vanishing operator is [12]

$$\mathcal{O}_{pv} = \frac{1}{\Lambda^2} X^\mu \epsilon_{\mu\nu\rho\sigma} \text{Tr}[F^{\nu\rho} \partial_\beta F^{\beta\sigma}]. \quad (9)$$

For non-Abelian fields $F_{\alpha\beta}^a$, covariant derivatives should be used to act on the field strengths. The covariant derivatives will give rise to higher point vertices, allowing decays to 3 or more standard model bosons.¹ For coupling to gluons, the higher point interactions have a sizable contribution to the production channel.

We will assume a higher-dimensional effective coupling to all gauge groups of the standard model, though for generality we will allow the couplings to be different. We will thus characterize the couplings by an energy scale Λ , and encode the relative strength of the coupling to $\text{SU}(2)_L$ and $\text{U}(1)_Y$ in relation to $\text{SU}(3)_{\text{QCD}}$ by C_1 and C_2 . The effective operators are thus given as

$$\mathcal{O}_s = \frac{1}{\Lambda_s} X G_{\mu\nu}^a G_a^{\mu\nu} + \frac{C_1}{\Lambda_s} X W_{\mu\nu}^i W_i^{\mu\nu} + \frac{C_2}{\Lambda_s} X B_{\mu\nu} B^{\mu\nu} \quad (10)$$

$$\mathcal{O}_{ps} = \frac{1}{\Lambda_{ps}} X G_{\mu\nu}^a \tilde{G}^{\mu\nu} + \frac{C_1}{\Lambda_{ps}} X W_{\mu\nu}^i \tilde{W}_i^{\mu\nu} + \frac{C_2}{\Lambda_{ps}} X B_{\mu\nu} \tilde{B}^{\mu\nu} \quad (11)$$

$$\mathcal{O}_v = \frac{1}{\Lambda_v^2} X^\mu G_{\mu\alpha}^a D_\beta G^{a\alpha\beta} + \frac{C_1}{\Lambda_v^2} X^\mu W_{\mu\alpha}^i D_\beta W^{i\alpha\beta} + \frac{C_2}{\Lambda_v^2} X^\mu B_{\mu\alpha} D_\beta B^{\alpha\beta} \quad (12)$$

$$\mathcal{O}_{pv} = \frac{1}{\Lambda_{pv}^2} X^\mu \tilde{G}_{\mu\alpha}^a D_\beta G^{a\alpha\beta} + \frac{C_1}{\Lambda_{pv}^2} X^\mu \tilde{W}_{\mu\alpha}^i D_\beta W^{i\alpha\beta} + \frac{C_2}{\Lambda_{pv}^2} X^\mu \tilde{B}_{\mu\alpha} D_\beta B^{\alpha\beta} \quad (13)$$

with $\tilde{F}_{\mu\nu} = \frac{1}{2} \epsilon_{\mu\nu\sigma\tau} F^{\sigma\tau}$. Since field strengths are parity even objects and $\epsilon_{\mu\nu\sigma\tau}$ is parity odd, we see that the X in Eq. (11) and Eq. (13) is a pseudoscalar and pseudovector, respectively.

III. PRODUCTION AND DECAY CHANNELS

Production at the LHC will be primarily through the channels gg , gq , $g\bar{q}$, and $q\bar{q}$. Vector boson fusion is also a viable production channel for the X [10], but will only become important when coupling to $\text{SU}(3)$ is small or zero. Thus we will not consider VBF as a production channel in this analysis, though we note that inclusion of this production channel will only add to the 2-jet cross section. We see (Fig. 1) that all but the gg partonic production channels require the presence of a spectator jet. If X is spin-1, the dominant $gg \rightarrow X$ production channel is forbidden for on-shell X ; thus spin-1 X is *always* produced with at least one accompanying jet. Since this dominant production channel is available to the spin-0 X , we should in principle be able to determine spin by simply comparing the zero-jet and one-jet cross sections for any observed fermiophobic resonance. We will return

¹ Extra terms arising from the covariant derivative will not affect two-body decay widths. They do, however, affect two-body branching fractions through their contribution to three-body widths, and so we use the full covariant derivatives in all of our couplings for event generation.

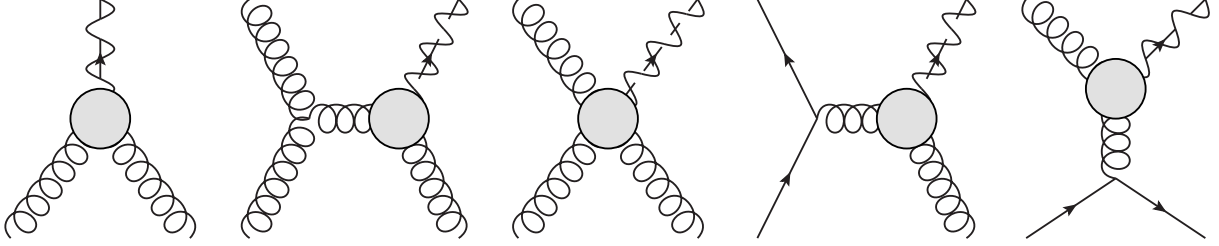


FIG. 1. Partonic production channels for the X

TABLE I. Tree-level production cross sections (in fb) for $X + 0$ -jet and $X + 1$ -jet, as calculated by MadGraph5 for $C_1 = 10$, $C_2 = 0$, and either $\Lambda = 50$ TeV (spin-0) or $\Lambda = \sqrt{10}$ TeV (spin-1). Cross sections for parity even and parity odd are identical for a spin-0 X . Jets are required to have $p_T \geq 50$ GeV.

m_X	500 GeV	1000 GeV	1500 GeV	2000 GeV
$\sqrt{s} = 8$ TeV				
$\sigma(pp \rightarrow X_{(p)s})$	4.70×10^2	3.38×10^1	4.31	6.82×10^{-1}
$\sigma(pp \rightarrow X_{(p)v})$	0	0	0	0
$\sigma(pp \rightarrow X_{(p)s} + j)$	2.71×10^2	2.69×10^1	4.03	7.04×10^{-1}
$\sigma(pp \rightarrow X_v + j)$	7.26×10^1	8.17	1.36	2.51×10^{-1}
$\sigma(pp \rightarrow X_{pv} + j)$	2.51×10^1	8.17	1.36	2.51×10^{-1}
$\sqrt{s} = 14$ TeV				
$\sigma(pp \rightarrow X_{(p)s})$	2.25×10^3	2.76×10^2	5.91×10^1	1.62×10^1
$\sigma(pp \rightarrow X_{(p)v})$	0	0	0	0
$\sigma(pp \rightarrow X_{(p)s} + j)$	1.53×10^3	2.53×10^2	6.40×10^1	1.94×10^1
$\sigma(pp \rightarrow X_v + j)$	7.48×10^2	1.32×10^2	3.72×10^1	1.24×10^1
$\sigma(pp \rightarrow X_{pv} + j)$	1.24×10^3	1.32×10^2	3.72×10^1	1.24×10^1

to this possibility in a later section. Interestingly, it turns out that the matrix element for the $gg \rightarrow Xg$ hard process also turns out to be zero if X is spin-1, so production occurs only through quark-gluon and quark-antiquark scattering.

We list the production cross sections for the different spin/parity assignments in Table I, as calculated in MadGraph5. Cross sections for production with zero and one jet are listed separately. We see, as expected, that the cross section for spin-1 X vanishes when there is no accompanying jet. We also see that production for spin-1 X is parity dependent at low masses, while for spin-0 X there is no noticeable dependence.

A. Decay Channels

Since the X is in general coupled to all gauge groups of the standard model, there is some non-zero branching fraction to both gluons and electroweak gauge bosons. If X decays via its coupling to gluons, the final state signal would lie in the multi-jet events; two or more jets for a spin-0 X and 4 or more jets for a spin-1 X (the matrix elements for $X \rightarrow gg, ggg$ vanish). As this is a difficult experimental analysis, we focus instead on electroweak decays, which lead to much cleaner signals at the LHC. Furthermore, since we want to study an on-

shell resonance, it is necessary that we can fully reconstruct the X from its decay products, and so we do not look in channels that contain neutrinos in the final state. We will look in the channels $X \rightarrow ZZ \rightarrow 4l$ (the so-called *golden channel*), $X \rightarrow Z\gamma \rightarrow 2l + \gamma$, and $X \rightarrow \gamma\gamma$ (the diphoton channel is forbidden for if X is spin-1).

Scalar decay widths are given by

$$\frac{\Gamma_s(WW)}{m_X} = \frac{C_1^2 m_X^2}{2\pi \Lambda^2} \sqrt{1 - \frac{4m_W^2}{m_X^2}} \left(1 - \frac{4m_W^2}{m_X^2} + 6\frac{m_W^4}{m_X^4}\right) \quad (14)$$

$$\frac{\Gamma_s(ZZ)}{m_X} = \frac{(C_1 \cos^2 \theta_w + C_2 \sin^2 \theta_w)^2 m_X^2}{4\pi \Lambda^2} \sqrt{1 - \frac{4m_Z^2}{m_X^2}} \left(1 - \frac{4m_Z^2}{m_X^2} + 6\frac{m_Z^4}{m_X^4}\right) \quad (15)$$

$$\frac{\Gamma_s(Z\gamma)}{m_X} = \frac{(C_1 - C_2)^2 \cos^2 \theta_w \sin^2 \theta_w m_X^2}{2\pi \Lambda^2} \left(1 - \frac{m_Z^2}{m_X^2}\right)^3 \quad (16)$$

$$\frac{\Gamma_s(\gamma\gamma)}{m_X} = \frac{(C_1 \sin^2 \theta_w + C_2 \cos^2 \theta_w)^2 m_X^2}{4\pi \Lambda^2} \quad (17)$$

$$\frac{\Gamma_s(gg)}{m_X} = \frac{2 m_X^2}{\pi \Lambda^2} \quad (18)$$

Note that the functional structures are identical to those of the standard model Higgs decay.

Pseudoscalar decay widths are given by

$$\frac{\Gamma_{ps}(WW)}{m_X} = \frac{C_1^2 m_X^2}{2\pi \Lambda^2} \left(1 - \frac{4m_W^2}{m_X^2}\right)^{3/2} \quad (19)$$

$$\frac{\Gamma_{ps}(ZZ)}{m_X} = \frac{(C_1 \cos^2 \theta_w + C_2 \sin^2 \theta_w)^2 m_X^2}{4\pi \Lambda^2} \left(1 - \frac{4m_Z^2}{m_X^2}\right)^{3/2} \quad (20)$$

$$\frac{\Gamma_{ps}(Z\gamma)}{m_X} = \frac{(C_1 - C_2)^2 \cos^2 \theta_w \sin^2 \theta_w m_X^2}{2\pi \Lambda^2} \left(1 - \frac{m_Z^2}{m_X^2}\right)^3 \quad (21)$$

$$\frac{\Gamma_{ps}(\gamma\gamma)}{m_X} = \frac{(C_1 \sin^2 \theta_w + C_2 \cos^2 \theta_w)^2 m_X^2}{4\pi \Lambda^2} \quad (22)$$

$$\frac{\Gamma_{ps}(gg)}{m_X} = \frac{2 m_X^2}{\pi \Lambda^2} \quad (23)$$

It is interesting to note that the scalar and pseudoscalar partial widths become equal as $m_{Z,W}/m_X \rightarrow 0$. This suggests that all information concerning the parity of the X is encoded in the longitudinal modes of the W and Z .

Vector decay widths are given by,

$$\frac{\Gamma_v(WW)}{m_X} = \frac{C_1^2 m_X^4 m_W^2}{48\pi \Lambda^4 m_X^2} \left(1 - \frac{4m_W^2}{m_X^2}\right)^{3/2} \quad (24)$$

$$\frac{\Gamma_v(ZZ)}{m_X} = \frac{(C_1 \cos^2 \theta_w + C_2 \sin^2 \theta_w)^2 m_X^4 m_Z^2}{96\pi \Lambda^4 m_X^2} \left(1 - \frac{4m_Z^2}{m_X^2}\right)^{3/2} \quad (25)$$

$$\frac{\Gamma_v(Z\gamma)}{m_X} = \frac{(C_1 - C_2)^2 \cos^2 \theta_w \sin^2 \theta_w m_X^4 m_Z^2}{96\pi \Lambda^4 m_X^2} \left(1 + \frac{m_Z^2}{m_X^2}\right) \left(1 - \frac{m_Z^2}{m_X^2}\right)^3 \quad (26)$$

TABLE II. Partial widths (in MeV), as calculated by MadGraph5, for $m_X = 500$ GeV, $C_1 = 10$, $C_2 = 0$, and either $\Lambda = 50$ TeV (spin-0) or $\Lambda = \sqrt{10}$ TeV (spin-1).

$V_1 V_2$	WW	ZZ	$Z\gamma$	$\gamma\gamma$	gg	3-body	$total$
Γ_s	680.2	190.1	128.8	21.73	31.83	89.63	1142
Γ_{ps}	677.2	188.6	128.8	21.73	31.83	90.00	1138
Γ_v	4.495	1.634	0.5762	0	0	0.3815	7.086
Γ_{pv}	4.037	1.416	0.5762	0	0	0.3516	6.381

Lastly, pseudovector decay widths are given by,

$$\frac{\Gamma_{pv}(WW)}{m_X} = \frac{C_1^2 m_X^4 m_W^2}{48\pi \Lambda^4 m_X^2} \left(1 - \frac{4m_W^2}{m_X^2}\right)^{5/2} \quad (27)$$

$$\frac{\Gamma_{pv}(ZZ)}{m_X} = \frac{(C_1 \cos^2 \theta_w + C_2 \sin^2 \theta_w)^2 m_X^4 m_Z^2}{96\pi \Lambda^4 m_X^2} \left(1 - \frac{4m_Z^2}{m_X^2}\right)^{5/2} \quad (28)$$

$$\frac{\Gamma_{pv}(Z\gamma)}{m_X} = \frac{(C_1 - C_2)^2 \cos^2 \theta_w \sin^2 \theta_w m_X^4 m_Z^2}{96\pi \Lambda^4 m_X^2} \left(1 + \frac{m_Z^2}{m_X^2}\right) \left(1 - \frac{m_Z^2}{m_X^2}\right)^3 \quad (29)$$

Again, we see that the parity-even and parity-odd widths become equal as $m_{Z,W}/m_X \rightarrow 0$.

In Table II, we list the widths (in MeV) to each channel for $m_X = 500$ GeV, $C_1 = 10$, $C_2 = 0$, and either $\Lambda = 50$ TeV (spin-0) or $\Lambda = \sqrt{10}$ TeV (spin-1). We see that for all cases the narrow width approximation is valid. To see that the narrow width approximation remains valid throughout our parameter space, we plot the contours of Γ_{tot}/m_X in Λ - m_X space for both spin-0 (Fig. 2) and spin-1 (Fig. 3). We neglect any contributions from three-body decays. We see that for spin-0, $\Gamma_{tot}/m_X < 10\%$ for a majority of the parameter space, though at large values of m_X/Λ the narrow width approximation may break down. In the case of a spin-1 X , the narrow width approximation holds over a much wider region of parameter space.

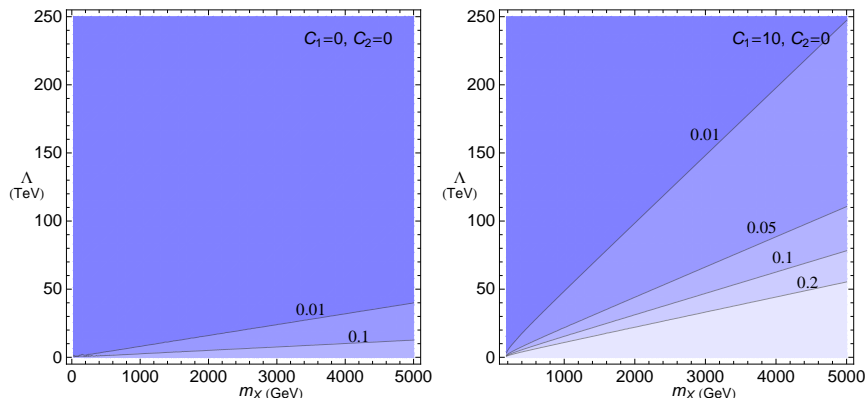


FIG. 2. Contours of Γ_{tot}/m_X for spin-0 X , for coupling only to gluons ($C_1 = C_2 = 0$) (left) and for coupling to SU(2) with $C_1 = 10$, $C_2 = 0$. For a vast majority of the parameter space width is less than 10% of the mass, and the narrow width approximation is valid.

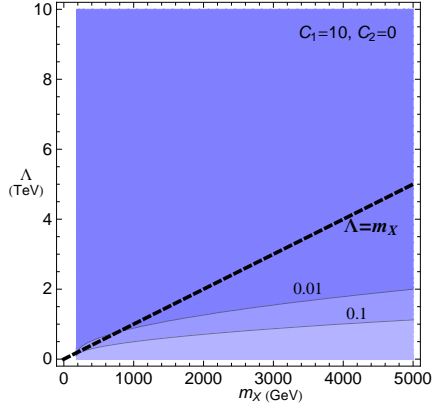


FIG. 3. Contours of Γ_{tot}/m_X for spin-1 X . Also shown is the line $\Lambda = m_X$, at which point the effective field theory description is naively expected to break down. For coupling to SU(2) with $C_1 = 10$ we find $\Gamma_{tot}/m_X \ll 1$ over a vast majority of the parameter space, and the narrow width approximation holds.

We can now calculate the branching fractions, again ignoring contributions from three-body decays, from Eqs. (14)-(29). The branching fractions for spin-0 X depend on two parameters, C_1 and C_2 . We illustrate this dependence in Fig. 4 by plotting branching fractions for a certain choice of C_1 and as a function of C_2/C_1 .

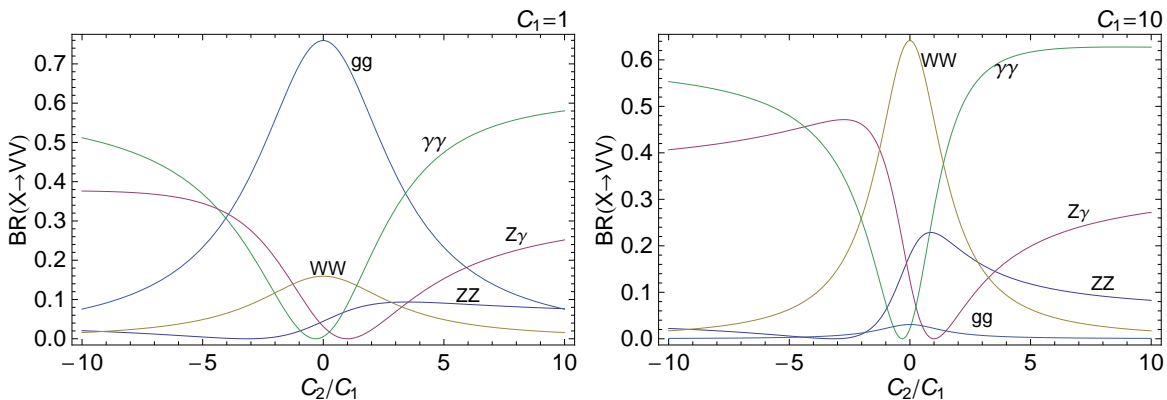


FIG. 4. X decay branching fractions when X is spin-0 as a function of C_2/C_1 . Here, $m_X = 500$ GeV and either $C_1 = 1$ (left panel) or $C_1 = 10$ (right panel).

For the spin-1 X , the branching fraction to gg (and $\gamma\gamma$) vanishes, and so the overall scale of the electroweak couplings in relation to the gluon coupling drops out. Thus the remaining branching fractions only depend on C_2/C_1 , and are constant with respect to overall scale Λ . These are shown in Fig. 5

Branching ratios in both cases are also dependent on m_X , but for $m_X \gtrsim 500$ GeV the dependence becomes negligible. Similarly, differences between parity even and parity odd become negligible.

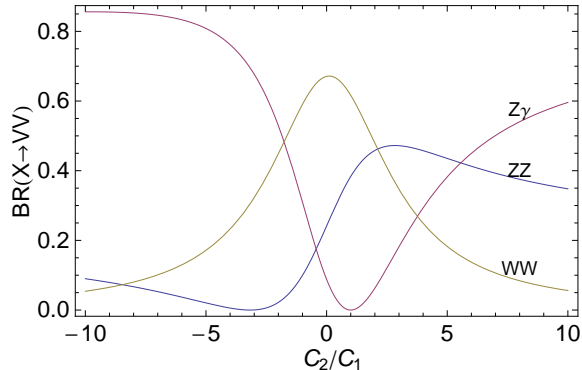


FIG. 5. X decay branching fractions for when X is spin-1 as a function of C_2/C_1 , for $m_X = 500$ GeV.

TABLE III. Three-body branching fractions, as calculated in MadGraph5, for $C_1 = 10$, $C_2 = 0$, and either $\Lambda = 50$ TeV (spin-0) or $\Lambda = \sqrt{10}$ TeV (spin-1).

$m_X =$	500 GeV	1000 GeV	1500 GeV	2000 GeV	10 TeV
X_s	0.078	0.154	0.207	0.24	0.436
X_{ps}	0.079	0.154	0.206	0.245	0.447
X_v	0.054	0.129	0.199	0.266	0.818
X_{pv}	0.055	0.129	0.199	0.267	0.816

B. Three-body decays

In the previous section, we ignored three-body decay widths due to the usual assumption that the reduction in phase space and extra coupling constant factors render these negligible. There are cases, however, where this assumption cannot be made. We show in Table III the three-body branching ratios for all four spin/parity assignments at five different masses. We see that when X is spin-0, the three-body branching fractions are small, but in general they are not negligible. More importantly, we see that if X is spin-1, the three-body decays strongly dominate for $m_X \gg m_{W,Z}$. This behavior arises again from the Landau-Yang theorem. For $m_X \gg m_{W,Z}$, the electroweak gauge bosons can be considered approximately massless, and the two-body decay becomes highly suppressed. We see this clearly in the vector and pseudovector three-body branching fractions for $m_X = 10$ TeV.

It is thus important to note that searches for two-body resonances will be ineffective for very massive fermiophobic spin-1 particles. Furthermore, any search for a three-body resonance will be complicated by the fact that, for electroweak decay products, full reconstruction using only leptons and photons is impossible. The only three-body electroweak decay modes for the X are W^+W^-Z and $W^+W^-\gamma$; purely leptonic decays will always produce missing momentum via neutrinos. Thus for full reconstruction we must rely on the hadronic channels, (either $X \rightarrow gq\bar{q}$ or hadronic decays of electroweak gauge bosons). Since a vector X must be produced with an associated jet, this signal will be contained within events containing 4 or more jets. Alternatively, a search can be performed in channels in which intermediate electroweak bosons are off-shell.

For $m_X \leq 2000$ GeV, the branching fractions to electroweak gauge bosons dominate, and

we may still be able to achieve discovery in the two-body decay channels. The remainder of this paper will focus on this possibility, and the possibility of distinguishing spin if a resonance is indeed observed.

IV. COLLIDER SIMULATION

As outlined above, we will generate event samples in which X is produced through the Xgg vertex and subsequently decays through electroweak couplings. We generate parton-level events in MadGraph5 [20], shower and hadronize the events in Pythia [21], and perform detector simulation using PGS4 [22] using the ATLAS detector card. To generate the model files for MadGraph, we have used the Mathematica package FeynRules [23], to which we feed the effective interaction operators, Eq. (10)-(13), as input. We generated events for collider energies of $\sqrt{s} = 8$ TeV and $\sqrt{s} = 14$ TeV.

For spin-0 X , we generate both $pp \rightarrow X$ and $pp \rightarrow Xj$ at the parton level, in order to include all possible production channels. These two processes are matched at the Pythia level using the MLM algorithm in order to avoid over counting between matrix element generated and ISR generated jet-containing events. For the spin-1 cases, events are generated solely from the 1-jet matrix element (which in this case is tree-level).

A. Cuts

The following reconstruction cuts will be applied for the three channels we study. These cuts are applied at the detector level.

- $X \rightarrow ZZ$

We require events to contain 4 charged leptons (e^\pm, μ^\pm) with $\eta \leq 2.5$. These must consist of two pairs of same-flavor opposite-sign leptons which each have invariant masses in the range $80 \text{ GeV} \leq m_{l+l-} \leq 100 \text{ GeV}$. The total invariant mass must lie within 10% of m_X .

- $X \rightarrow Z\gamma$

We require events to contain a photon as well as 2 same-flavor opposite-sign leptons ($\eta \leq 2.5$) whose invariant mass lies in the range $80 \text{ GeV} \leq m_{l+l-} \leq 100 \text{ GeV}$. The two leptons and photon then must have a total invariant mass which lies within 10% of m_X .

- $X \rightarrow \gamma\gamma$

We require events to contain 2 photons ($\eta \leq 2.5$) which reconstruct to invariant mass within 10% of m_X .

In addition to these cuts, a number of standard isolation cuts are applied at the MadGraph level, including requiring $\Delta R > 0.4$ for any pair of particles. At this point we do not impose any cuts on the jet structure of the events.

B. Background

We generate background events using the same MadGraph5 simulation chain. For the vast majority of events where a lepton pair has an invariant mass between 80 – 100 GeV, the leptons arise from the decay of a Z boson. Other sources of lepton pairs satisfying the cuts (including lepton misidentification) are insignificant and can be ignored. For the ZZ and $Z\gamma$ background channels, we use 0-jet and 1-jet matrix elements, which are matched using the MLM algorithm. For the $\gamma\gamma$ channel, we use only the 0-jet matrix element. Cross sections for these channels, after imposing the above mentioned cuts in each X -mass window, are given in Table IV at LHC energies of 8 TeV and 14 TeV (see also [24, 25]).

TABLE IV. Inclusive cross sections (in fb) for standard model background in the ZZ , $Z\gamma$, and $\gamma\gamma$ channels, after reconstruction cuts in each total invariant mass window.

		m_X			
		500 GeV	1000 GeV	1500 GeV	2000 GeV
8 TeV	$\sigma_{BG}(pp \rightarrow ZZ \rightarrow l^+l^-l^+l^-)$	2.09×10^{-1}	7.35×10^{-3}	1.87×10^{-4}	2.16×10^{-5}
	$\sigma_{BG}(pp \rightarrow Z\gamma \rightarrow l^+l^-\gamma)$	3.93	2.98×10^{-1}	2.55×10^{-2}	2.93×10^{-3}
	$\sigma_{BG}(pp \rightarrow \gamma\gamma)$	1.80×10^1	1.42	2.08×10^{-1}	4.66×10^{-2}
14 TeV	$\sigma_{BG}(pp \rightarrow ZZ \rightarrow l^+l^-l^+l^-)$	4.41×10^{-1}	2.45×10^{-2}	1.90×10^{-3}	1.61×10^{-4}
	$\sigma_{BG}(pp \rightarrow Z\gamma \rightarrow l^+l^-\gamma)$	8.42	4.16×10^{-1}	1.09×10^{-1}	2.72×10^{-2}
	$\sigma_{BG}(pp \rightarrow \gamma\gamma)$	3.65×10^1	2.79	8.73×10^{-1}	3.27×10^{-1}

V. COLLIDER REACH

Since the narrow width approximation holds, the number of signal events in a given channel and at a given luminosity \mathcal{L} depends on the coupling constants C_1 and C_2 only though the final state branching fractions. If we denote by σ_{prod} the cross-section for the production process $pp \rightarrow X + (0 \text{ and/or } 1 - \text{jet})$, and by ϵ the fraction of such events which pass the analysis cuts in any channel, then the number of signal events is given by

$$N_{sig} = \sigma_{\text{prod}} \times \epsilon \times BR(X \rightarrow VV) \times \mathcal{L} \\ \propto \Lambda^{-n} \times BR(X \rightarrow VV) \times \mathcal{L} \quad (30)$$

where $n = 2$ for spin-0, and $n = 4$ for spin-1. For a discovery, we will require a 5σ (Gaussian equivalent) excess of signal events over background events satisfying the same cuts, and we require at least 5 signal events. With Eq. (30) in mind, we define the LHC reach for any integrated luminosity in terms of the quantity

$$R_{VV} \equiv \Lambda/[BR(X \rightarrow VV)]^{1/n}. \quad (31)$$

We find the reach for 10 fb^{-1} and 30 fb^{-1} at center of mass energy of $\sqrt{s} = 8 \text{ TeV}$, and 100 fb^{-1} at $\sqrt{s} = 14 \text{ TeV}$. For the scalar and vector cases, the LHC reach is plotted against m_X in Fig. 6. We plot the inclusive $X \rightarrow ZZ$ channel (both 0 and 1-jet events) and the inclusive $X \rightarrow Z\gamma$ channels separately. The reach plots for the pseudoscalar and pseudovector case are essentially identical to the scalar and vector cases, respectively. We see that in both channels, we can probe higher scales in the spin-0 case, which is expected

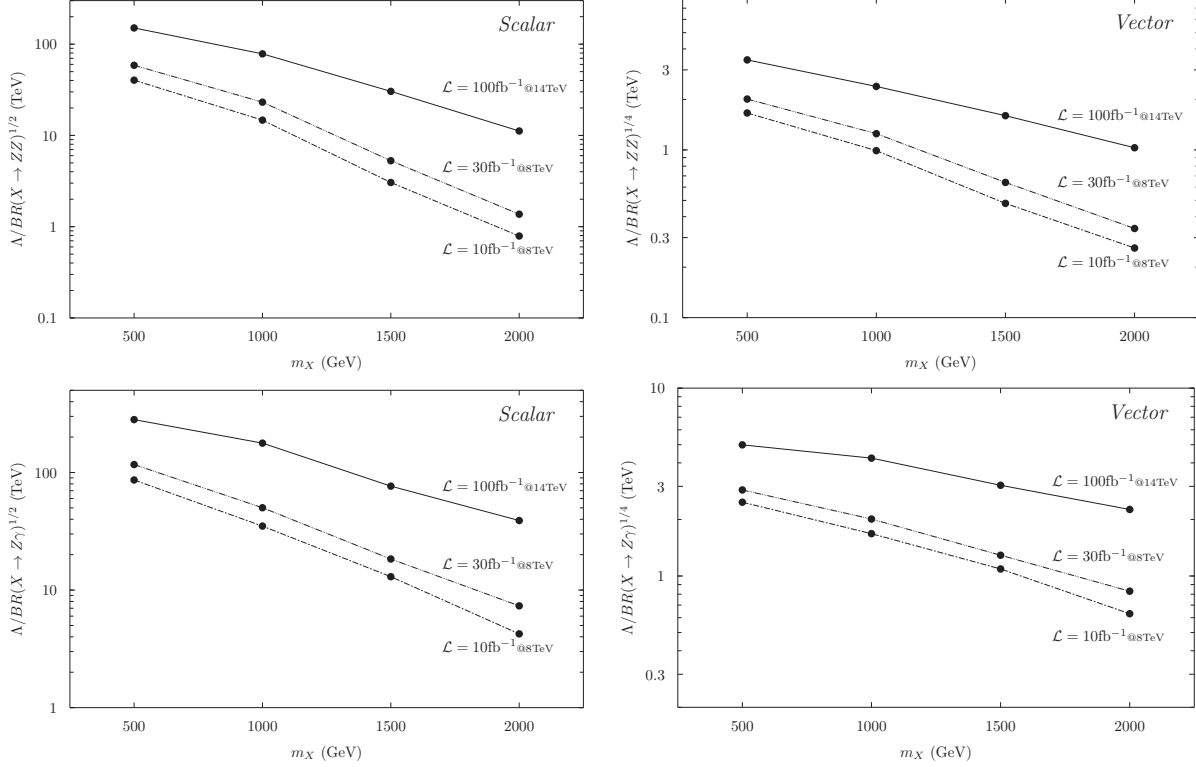


FIG. 6. Collider reach for both ZZ (top) and $Z\gamma$ (bottom) channels. Spin-0 X is shown at left, spin-1 X at right. The reach plots for the parity odd bosons are essentially identical to their parity even counterparts.

from the additional Λ^2 suppression coming from the dimension 6 operators coupling a spin-1 fermiophobic boson to the standard model. We also note that the $Z\gamma$ channel is generally a better probe despite the higher backgrounds. This is mainly due to the small $Z \rightarrow l^+l^-$ branching fraction and the reconstruction cuts present in the ZZ channel.

In addition, we show in Fig. 7 the reach for the $\gamma\gamma$ channel, present only for spin-0 X . Current LHC data can probe well into the hundreds-of-TeV range.

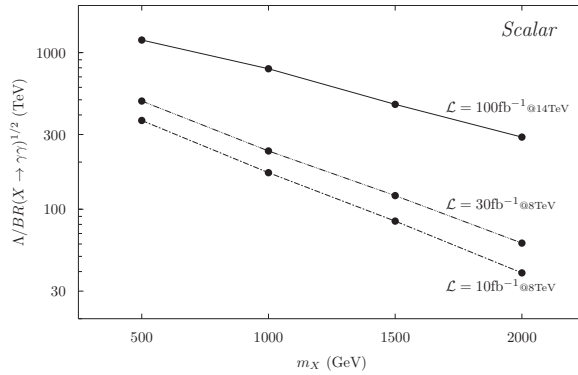


FIG. 7. Collider reach for both $\gamma\gamma$ channel, which is present only for spin-0 X .

Note that we have not accounted for NLO QCD corrections to the X production cross section. The associated K -factors are usually greater than one, indicating that a correct

treatment of NLO effects would likely increase the LHC reach.

A. Spin Determination

It is clear from the reach plots of the previous section that the simplest way to distinguish a spin-0 resonance from spin-1 is to look to the $\gamma\gamma$ channel. If there is an observation in the $\gamma\gamma$ channel, with or without a corresponding observation in ZZ or $Z\gamma$, the Landau-Yang theorem implies that the decaying particle is not spin-1.

There are cases, however, where a spin-0 X will not decay to two photons. We see from Fig. 4 and Eq. (17) that the branching ratio $BR(X \rightarrow \gamma\gamma)$ drops to zero for $C_2/C_1 = -\tan^2\theta_w$ (an explicit model where this occurs is exhibited in the Appendix). The electroweak decay channels for the spin-0 and spin-1 X are in this case identical. We must in these cases resort to an alternative method of determining spin.

Another way of distinguishing between spin-0 and spin-1 resonances is from the presence of extra jets; the 0-jet process $pp \rightarrow X \rightarrow ZZ, Z\gamma$ is possible if X is spin-0, but not if it is spin-1. As we saw, we can define the LHC reach for X (spin-0) in terms of the quantity $R_{VV} = \Lambda/BR(X \rightarrow VV)^{1/2}$. We thus see that a search in the ZZ or $Z\gamma$ channel with zero extra jets will be more promising than a search in the $\gamma\gamma$ channel if

$$\frac{R_{ZZ,Z\gamma}(0\text{-jet})}{R_{\gamma\gamma}} \left[\frac{BR(X \rightarrow ZZ, Z\gamma)}{BR(X \rightarrow \gamma\gamma)} \right]^{\frac{1}{2}} > 1. \quad (32)$$

The ratios $BR(X \rightarrow ZZ)/BR(X \rightarrow \gamma\gamma)$ and $BR(X \rightarrow Z\gamma)/BR(X \rightarrow \gamma\gamma)$ depend only on the quantities m_X and C_2/C_1 . Having determined $R_{ZZ}(m_X)$ and $R_{Z\gamma}(m_X)$ for the 0-jet sample from the generated signal and background events, one can determine the range of C_2/C_1 (for any m_X) over which the ZZ or $Z\gamma$ 0-jet search provides better prospects for discovery than the $\gamma\gamma$ channel. These ranges are plotted in Fig. 8; note that these ranges would not change significantly after the LHC energy and luminosity upgrade.

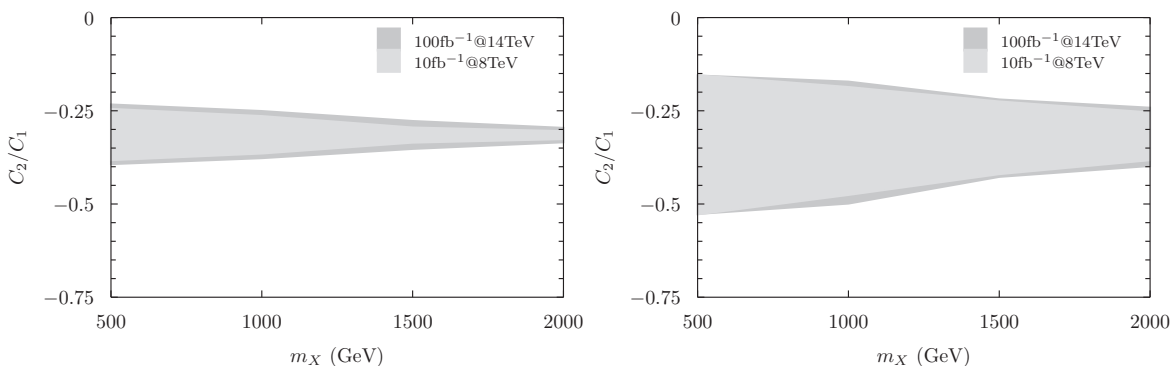


FIG. 8. Range of C_2/C_1 for which a ZZ -channel search (left) or a $Z\gamma$ -channel (right) search is more promising than a diphoton search.

Thus far, our analysis has focused on strategies for determining if X is not spin-1. One might ask the converse question: does the appearance of an excess in ZZ and/or $Z\gamma$ events with one extra jet, unaccompanied by an excess in 0-jet events or $\gamma\gamma$ events, necessarily imply the X resonance is spin-1? Essentially, this amounts to the question of whether or

not a spin-0 resonance can produce an excess in 1-jet events, without also producing a statistically significant excess in 0-jet events or $\gamma\gamma$ events.

We can determine this by comparing the LHC reach for 0-jet events to the reach for 1-jet events in the ZZ or $Z\gamma$ events, assuming X is spin-0. If the reaches are comparable, then a spin-0 X coupling to the standard model in such a way as to produce a 5σ excess in ZZ or $Z\gamma$ events with 1 extra spectator jet would, for similar luminosity, also produce an excess in events with no spectator jets. An observed 5σ excess in 1-jet events without some excess in 0-jet events would imply that X is not spin-0.

In Fig. 9 we plot $R_{VV}(0\text{-jet})/R_{VV}(1\text{-jet})$ as a function of m_X for the ZZ and $Z\gamma$ channels (assuming X is spin-0). From this plot, we see that for much of the range, an observation of a resonance with one spectator jet, but an absence of a excess with zero spectator jets, is sufficient to demonstrate that the resonance is not spin-0. Furthermore, we see that this conclusion is largely independent of the collider energy, luminosity, and decay channel studied. We also show (Fig. 10) $R_{VV}(0\text{-jet})/R_{VV}(1\text{-jet})$ for the case of a spin-1 X (in this

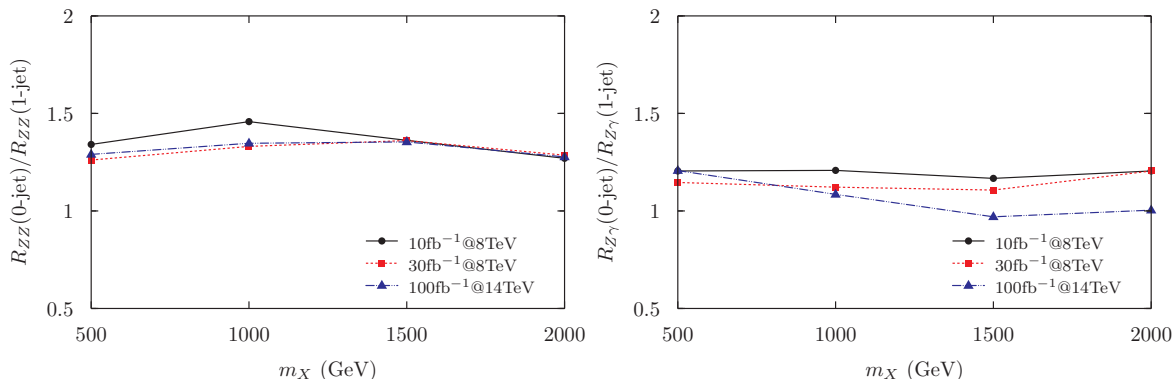


FIG. 9. Ratio of reaches $R_{VV}(0\text{-jet})/R_{VV}(1\text{-jet})$ for $X \rightarrow ZZ$ (left) and $X \rightarrow Z\gamma$ (right) in the case of spin-0 X . We see that if the resonance is spin-0, we expect a similar number of 0-jet and 1-jet events.

case, the number of signal events is proportional to R^{-4}). As expected, we see that an observation in the 0-jet channel without a corresponding observation in the 1-jet channel is sufficient to demonstrate that the resonance is not spin-1.

VI. CONCLUSIONS

The existence of exotic fermiophobic bosons is well-motivated theoretically. These types of bosons could reveal themselves as resonances which decay to two or more SM bosons at the LHC. We have established the efficacy of the LHC in probing models of this type, and demonstrated the viability of two methods for determining spin. The existence of a diphoton decay channel establishes that the resonance is not spin-1, as is well-known. When a boson does not decay to two photons, spin can be determined through an inspection of the jet structure of the signal events. Over much of the parameter space, a discovery and a spin determination can be achieved in as few as 5 events, thus requiring far fewer statistics than alternative methods of spin determination (*e.g.* analyses of angular distributions of decay products).

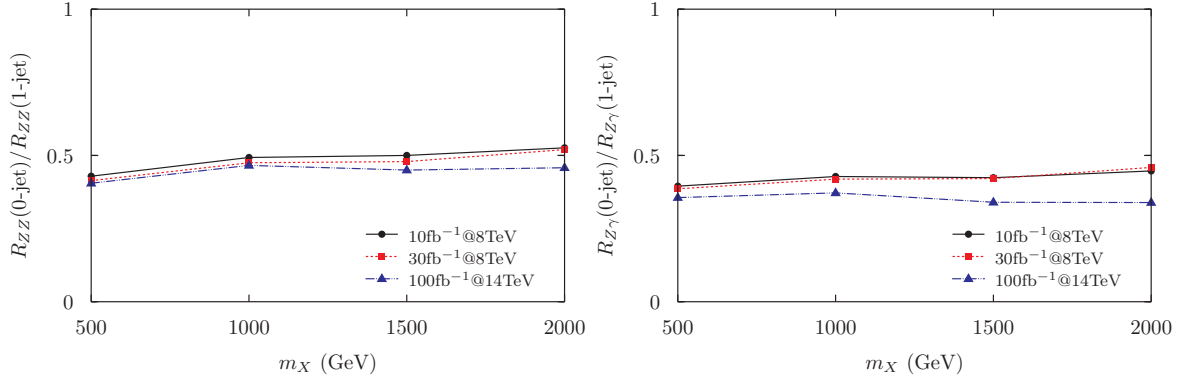


FIG. 10. Ratio of reaches $R_{VV}(0\text{-jet})/R_{VV}(1\text{-jet})$ for $X \rightarrow ZZ$ (left) and $X \rightarrow Z\gamma$ (right) in the case of spin-1 X . We see that if the resonance is spin-1, we expect to many 1-jet events and very few 0-jet events.

The LHC has already discovered a new boson, and the existence of diphoton decays shows definitively that this new particle is not spin-1. We have shown that the LHC has very good prospects for discovering fermiophobic bosons in the near future, even if they are relatively heavy, or are only coupled to the standard model by higher dimension effective operators which are heavily suppressed. For example, a 100 fb^{-1} run of the LHC at 14 TeV could find 5σ evidence for a scalar with $m_X \sim 2 \text{ TeV}$, coupled to the standard model by effective operators suppressed by a mass scale $\sim 300 \text{ TeV}$. The reason for this large reach is that a fermiophobic boson can be produced from gluon couplings, but observed through electroweak decays, a channel which is ideal for detection at the LHC. In particular, the diphoton channel is clearly the most promising, as the signal is very clean and the background is very small.

But one typically expects an electrically neutral boson to have a very small branching fraction for decay to $\gamma\gamma$. This is the case for the 125 GeV boson discovered at the LHC. Fermiophobic scalars are a major contrary example; the branching fraction for diphoton decay can easily be $\mathcal{O}(1)$. One can see why such large $X \rightarrow \gamma\gamma$ branching fractions are allowed by considering a high-energy theory where the fermiophobic boson X couples to standard model gauge bosons only through loops of heavy fermions and scalars which are charged under standard model gauge groups. In this scenario, since all decays arise from one-loop diagrams, the $X \rightarrow \gamma\gamma$ branching fraction can be comparable to that of other channels. This behavior is markedly different from other scenarios in which some decays to standard model particles occur at tree-level. Fermiophobic bosons are thus one of the most interesting prospects for future discovery at an upgraded LHC.

Although the methods we have discussed here are applicable for spin determination, it is clear from our results that parity information is generally not encoded in jet number distributions. Alternative methods must be used to determine the parity of the couplings, which would give clues to the nature of the underlying physics of the new resonance.

Acknowledgments

We are grateful to B. Thomas and J. Alwall for useful discussions. The work of J. K. and D. Y. is supported in part by Department of Energy grant DE-FG02-04ER41291. The work of A.R. is supported in part by NSF grant PHY-0970173.

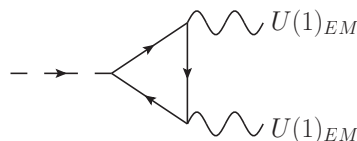
Appendix A: Vanishing $BR(X \rightarrow \gamma\gamma)$

The condition that $C_2 = -C_1 \tan^2 \theta_w$, which is necessary for a vanishing branching ratio to two photons, can arise naturally as follows. Let us assume that the X couples to electroweak gauge bosons through triangle diagrams involving extra heavy fermions. In this model there are two extra vector-like fermion multiplets. One is an $SU(2)$ doublet,

$$\begin{pmatrix} a \\ b \end{pmatrix}, \text{ with } Y = -1,$$

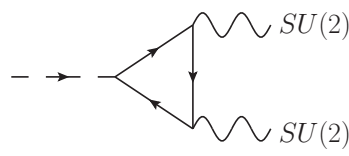
which couples to X through a Yukawa interaction with coupling constant λ_1 . The other is an $SU(2)$ singlet, c , with $Y = -2$ and which couples to X through a Yukawa interaction with coupling constant λ_2 . The electric charge ($Q = T^3 + Y/2$) of b and c is $-e$ while the charge of the a is zero.

Let us first consider the coupling to two photons. Only b and c will contribute to the loop, so the amplitude is proportional to



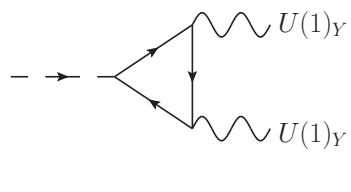
A triangle diagram with an incoming line on the left and two outgoing wavy lines on the right. The top and bottom wavy lines are labeled $U(1)_{EM}$. The diagram is associated with the expression $\propto \lambda_1(-e)^2 + \lambda_2(-e)^2$.

We see that for the $X\gamma\gamma$ coupling to vanish, we must have $\lambda_1 = -\lambda_2$. Now, we look to the couplings to the $SU(2)$ and $U(1)_Y$ gauge bosons. For $SU(2)$, only the doublet runs in the loop, and we have



A triangle diagram with an incoming line on the left and two outgoing wavy lines on the right. The top and bottom wavy lines are labeled $SU(2)$. The diagram is associated with the expression $\propto \lambda_1 g^2 \text{Tr}(t_i t_j)$ and $\propto \frac{1}{2} \lambda_1 g^2$.

We can identify this factor as our coefficient C_1 . For $U(1)_Y$, all three particles flow in the loop, and we find



A triangle diagram with an incoming line on the left and two outgoing wavy lines on the right. The top and bottom wavy lines are labeled $U(1)_Y$. The diagram is associated with the expression $\propto \lambda_1 g'^2 (-\frac{1}{2})^2 + \lambda_1 g'^2 (-\frac{1}{2})^2 + \lambda_2 g'^2 (-1)^2$, $= \frac{1}{2} \lambda_1 g'^2 + \lambda_2 g'^2$, and $= -\frac{1}{2} \lambda_1 g'^2$.

where in the last line we replaced $\lambda_2 = -\lambda_1$. This coefficient can be identified with C_2 . Since $g' = g \tan \theta_w$, we see that $C_2 = -C_1 \tan^2 \theta_w$ as needed.

The above argument is strictly only valid if the particles coupling to the X — a , b , and c — have identical masses. If this condition is relaxed, then the diphoton coupling will vanish only for $\lambda_1 \approx -\lambda_2$.

[1] B. Holdom, Phys. Lett. B **166**, 196 (1986).

- [2] F. del Aguila, M. Masip and M. Perez-Victoria, Nucl. Phys. B **456**, 531 (1995) [arXiv:hep-ph/9507455].
- [3] K. R. Dienes, C. F. Kolda and J. March-Russell, Nucl. Phys. B **492**, 104 (1997) [arXiv:hep-ph/9610479].
- [4] P. Anastasopoulos, M. Bianchi, E. Dudas and E. Kiritsis, JHEP **0611**, 057 (2006) [arXiv:hep-th/0605225].
- [5] J. Kumar and J. D. Wells, Phys. Rev. D **74**, 115017 (2006) [arXiv:hep-ph/0606183].
- [6] D. Feldman, Z. Liu and P. Nath, JHEP **0611**, 007 (2006) [arXiv:hep-ph/0606294].
- [7] W. F. Chang, J. N. Ng and J. M. S. Wu, Phys. Rev. D **74**, 095005 (2006) [Erratum-ibid. D **79**, 039902 (2009)] [arXiv:hep-ph/0608068].
- [8] W. F. S. Chang, J. N. Ng and J. M. S. Wu, Phys. Rev. D **75**, 115016 (2007) [arXiv:hep-ph/0701254].
- [9] D. Feldman, Z. Liu and P. Nath, Phys. Rev. D **75**, 115001 (2007) [arXiv:hep-ph/0702123].
- [10] J. Kumar, A. Rajaraman and J. D. Wells, Phys. Rev. D **77**, 066011 (2008) [arXiv:0707.3488 [hep-ph]].
- [11] I. Antoniadis, A. Boyarsky, S. Espahbodi, O. Ruchayskiy, J. D. Wells, Nucl. Phys. **B824**, 296-313 (2010). [arXiv:0901.0639 [hep-ph]].
- [12] J. Bramante, R. S. Hundi, J. Kumar, A. Rajaraman, and D. Yaylali, Phys. Rev. **D84** (2011) [arXiv:1106.3819 [hep-ph]].
- [13] F. Bach and T. Ohl, Phys. Rev. D **85**, 015002 (2012) [arXiv:1111.1551 [hep-ph]].
- [14] M. A. Diaz and T. J. Weiler, hep-ph/9401259; A. G. Akeroyd, Nucl. Phys. B **544**, 557 (1999) [hep-ph/9806337]; L. Brucher and R. Santos, Eur. Phys. J. C **12**, 87 (2000) [hep-ph/9907434]; E. Gabrielli and B. Mele, arXiv:1112.5993 [hep-ph]; E. Gabrielli, B. Mele and M. Raidal, Phys. Lett. B **716**, 322 (2012) [arXiv:1202.1796 [hep-ph]]; E. L. Berger, Z. Sullivan and H. Zhang, Phys. Rev. D **86**, 015011 (2012) [arXiv:1203.6645 [hep-ph]]; E. Gabrielli, K. Kannike, B. Mele, A. Racioppi and M. Raidal, arXiv:1204.0080 [hep-ph]; A. N. Jourjine, arXiv:1208.1867 [hep-ph].
- [15] V. Lemaître [ALEPH, DELPHI, L3 and OPAL Collaboration]; [CDF and D0 and Tevatron New Higgs Working Group Collaborations], arXiv:1109.0576 [hep-ex]; A. Collaboration *et al.* [ATLAS Collaboration], arXiv:1205.0701 [hep-ex]; S. Chatrchyan *et al.* [CMS Collaboration], arXiv:1207.1130 [hep-ex].
- [16] P. J. Fox, D. Tucker-Smith, N. Weiner, [arXiv:1104.5450 [hep-ph]].
 G. F. Giudice, R. Rattazzi and J. D. Wells, Nucl. Phys. B **595**, 250 (2001) [hep-ph/0002178].
 W. D. Goldberger and M. B. Wise, Phys. Lett. B **475**, 275 (2000) [hep-ph/9911457].
 C. Csaki, M. L. Graesser and G. D. Kribs, Phys. Rev. D **63**, 065002 (2001) [hep-th/0008151].
 W. D. Goldberger, B. Grinstein and W. Skiba, Phys. Rev. Lett. **100**, 111802 (2008) [arXiv:0708.1463 [hep-ph]].
 A. De Rujula, J. Lykken, M. Pierini, C. Rogan and M. Spiropulu, Phys. Rev. D **82**, 013003 (2010) [arXiv:1001.5300 [hep-ph]].
 I. Low and J. Lykken, JHEP **1010**, 053 (2010) [arXiv:1005.0872 [hep-ph]].
 H. Davoudiasl, T. McElmurry and A. Soni, Phys. Rev. D **82**, 115028 (2010) [Erratum-ibid. D **86**, 039907 (2012)] [arXiv:1009.0764 [hep-ph]].
 D. Bertolini and M. McCullough, arXiv:1207.4209 [hep-ph].
 U. De Sanctis, M. Fabbrichesi and A. Tonerio, Phys. Rev. D **84**, 015013 (2011) [arXiv:1103.1973 [hep-ph]].
 W. Bernreuther, P. Gonzalez and M. Wiebusch, Eur. Phys. J. C **69**, 31 (2010) [arXiv:1003.5585]

- [hep-ph].
Y. Gao, A. V. Gritsan, Z. Guo, K. Melnikov, M. Schulze and N. V. Tran, Phys. Rev. D **81**, 075022 (2010) [arXiv:1001.3396 [hep-ph]].
L. M. Carpenter and J. Goodman, arXiv:1205.5555 [hep-ph].
- [17] L. D. Landau, Dokl. Akad. Nauk., USSR **60**, 207 (1948); C. N. Yang, Phys. Rev. **77**, 242 (1950).
- [18] W. Y. Keung, I. Low and J. Shu, Phys. Rev. Lett. **101**, 091802 (2008) [arXiv:0806.2864 [hep-ph]].
- [19] S. Chatrchyan *et al.* [CMS Collaboration], Phys. Lett. B **716**, 30 (2012) [arXiv:1207.7235 [hep-ex]]; G. Aad *et al.* [ATLAS Collaboration], Phys. Lett. B **716**, 1 (2012) [arXiv:1207.7214 [hep-ex]].
- [20] J. Alwall, M. Herquet, F. Maltoni, O. Mattelaer, T. Stelzer, [arXiv:1106.0522 [hep-ph]].
- [21] T. Sjostrand, S. Mrenna and P. Z. Skands, JHEP **0605**, 026 (2006) [arXiv:hep-ph/0603175].
- [22] PGS – Pretty Good Simulator, <http://www.physics.ucdavis.edu/~conway/research/software/pgs/pgs4-general.html>.
- [23] N. Christensen and C. Duhr, Comput.Phys.Commun. **180** (2009) [arXiv:0806.4194v1 [hep-ph]].
- [24] U. Baur and E. W. N. Glover, Nucl. Phys. B **339**, 38 (1990).
- [25] U. Baur, E. W. N. Glover and J. J. van der Bij, Nucl. Phys. B **318**, 106 (1989).